MATERIALS CHEMISTRY FRONTIERS

RESEARCH ARTICLE

View Article Online
View Journal | View Issue

Cite this: *Mater. Chem. Front.*, 2024, **8**, 2859

Unsymmetrical substituted steric terfluorenes for solution-processed narrowband deep-blue organic light-emitting diodes with CIE_y = 0.06†

Ningning Yu,‡[a] Wenyu Chen,‡[a] Mengyuan Li,‡[a] Yingru Lin,[a] Xinyu Du,[a] Yingying Zheng,[a] Jing Yang,[a] Wenxin Huang,[a] Zhiqiang Zhuo,[a] Chuanxin Wei,[b] Xiang An,[a] Yamin Han,*[a] Lubing Bai,[a] Jiewei Li,[a] Xuehua Ding,[a] Heyuan Liu,*[c] Man Xu,[b] Wei Huang[ab] and Jinyi Lin*[a]

Multiple-site functionalization of deep-blue light-emitting conjugated molecules can not only optimize photo-electrical processing to obtain robust electroluminescent behavior but also enhance the film-forming ability to manufacture large-area film *via* solution processing technology. Herein, we demonstrate a pendant side-functionalization to prepare a series of unsymmetrical substituted steric terfluorenes (**MC8** and **MC6Cz**) *via* originally introducing the alkoxy and carbazole group at the 4-position of fluorene segments for the narrowband ultra-deep-blue solution-processed organic light-emitting diodes (OLEDs). Both materials exhibited an ultra-deep-blue emission with CIE coordinates of (0.16, 0.06) and PLQY efficiencies of ~60% due to the single-molecular exciton behavior without polariton formation, confirmed by the time-resolved transient spectroscopy. Interestingly, compared to the **MC8**, **MC6Cz** films present stable deep-blue emission without obvious green-band emission when thermally annealed in the air or irradiated for 3 hours under UV light, attributed to the self-encapsulation of the pendant carbazole group. Finally, **MC6Cz**-based OLEDs exhibited a narrowband ultra-deep-blue emission, a high brightness at low current density, with a high external quantum efficiency (EQE) of 1.17% and CIE coordinates of (0.16, 0.06). All the above results confirm that the introduction of the Cz group inhibits the aggregation between molecular main chains, realizing the single molecular mechanism of exciton behavior, establishing the two-dimensional carrier transport channel, and improving the morphology, spectral stability and efficiency of the material, which are conducive to the realization of efficient and stable solution-processed deep-blue light-emitting devices.

Received 20th April 2024,
Accepted 3rd June 2024

DOI: 10.1039/d4qm00332b

rsc.li/frontiers-materials

Introduction

Over the last decades, light-emitting conjugated materials (LCMs) have been widely applied in display and solid-lighting fields, associated with their efficient emission, easy structural modification, and potential flexible mechanical and printed properties.[1–6] To achieve the high quality of the three primary colours (blue, green and red) from organic light-emitting diodes (OLEDs) is the prerequisite to improve the colour-producing ability of the screen and color-rendering index (CRI) of solid-state lighting source.[5–9] Compared to the red and green ones, deep-blue LCMs always show a low emission efficiency, low charge density and mobility, and unstable emission, which result in low performance, low colour purity and operation lifetime of OLEDs due to their intrinsic wide bandgap (Scheme 1).[10] Defect structures with a narrow bandgap, including the chemical and physical ones, are easily formed in solid states, which will act as a center to trap high band exciton and cause the formation of multi-excited states.[11] This diverse and complicated photophysical processing, such as the excimer emission and self-absorption, is seriously undesirable for deep-blue OLEDs.[10,12–18] Especially, due to the complicated rheological properties and intermolecular

[a] *Key Laboratory of Flexible Electronics (KLoFE) and Institute of Advanced Materials (IAM) Nanjing Tech University (Nanjing Tech), 30 South Puzhu Road, Nanjing 211816, China. E-mail: iamjylin@njtech.edu.cn, liuheyuan123@upc.edu.cn, iamymhan@njtech.edu.cn*

[b] *State Key Laboratory of Organic Electronics and Information Displays & Institute of Advanced Materials (IAM), Nanjing University of Posts & Telecommunications, 9 Wenyuan Road, Nanjing 210023, China*

[c] *School of Materials Science and Engineering, Institute of New Energy, College of Science, China University of Petroleum (East China), Qingdao, Shandong, 266580, China*

† Electronic supplementary information (ESI) available. See DOI: https://doi.org/10.1039/d4qm00332b

‡ Ninging Yu, Wenyu Chen and Mengyuan Li are contributed equally to this work.

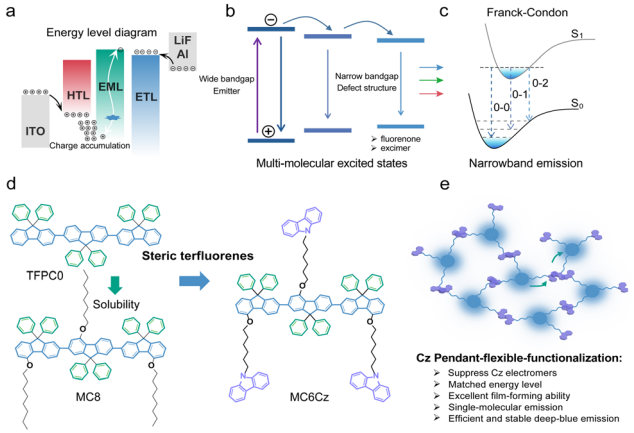

Scheme 1 Molecular design principle of unsymmetrical substituted steric terfluorenes *via* pendant side-functionalization. (a) Energy level diagram of traditional OLED based on terfluorenes.[11,29] (b) Undesirable energy transfer from wide bandgap emission center to narrowband defect structure, which results in a low efficiency and color purity of deep-blue emission.[30] (c) To suppress the formation of the charge transfer (CT) state can reduce the structural distortion and present a narrowband emission. The introduction of steric hindrance groups inhibits molecular aggregation and induces narrowband emission.[31] (d) Different pendants of steric terfluorenes. Schematic diagram of unsymmetrical substitution of steric terfluorenes *via* carbazole pendant functionalization at 4-position. (e) Efficient intermolecular charge transport in the Cz pendant functionalized terfluorene. The pendant Cz group at the unsymmetrical 4-site substitution of fluorene monomers can act as a charge transport station to enhance the film conductivity, although there is an extremely weak intermolecular π interaction and electron coupling.

deposition, heterogeneous films, consisting of parent individual chromophore and defect aggregate, are reasonably prepared *via* solution processing technology, which induces a lower performance, stability and repetitiveness than deposited OLEDs.[9,19–24] Saturated deep-blue emitters with a $CIE_y < 0.06$ are highly necessary to fulfill the production of the full-colour display (WOLEDs),[10,25–27] which is still rare for the phosphorescent and TADF electroluminescence (EL).[28] Therefore, it is urgent to design and prepare novel efficient and stable LCPs with a narrowband deep-blue emission toward OLEDs.

Similar to the industrial pulse assembly lines, modular production of LCMs have a series of advantages, such as precisely tenable electronic structure, controllable structural modification, and low-cost manufacture, analogous to Lego.[32,33] In general, LCMs consists of some typical conjugated segments, such as p- or n-type, and π-bridge units, that former two group can precisely tune the electronic structure and bangap to modulate the emission color and charge behavior, and the latter always control the intramolecular charge transfer and electron delocalization toward the optimization of the photophysical and electrical property.[10,33] Up to date, a series of p- and π-bridge moieties, such as anthracene, pyrene, dimesitylborane and fluorene phenanthroimidazole, are developed to manufacture deep-blue fluorescent LCMs.[10,25,29] Among them, fluorene is a common and universal segment to build high efficiency deep-blue LCM, due to its intrinsic multi-sites structural functionalization, wide bandgap and deep-blue emission for the light-emitting devices.[10,29,33] However, the traditional fluorene-based derivatives always suffer from poor color purity and low efficiency of deep-blue emission, especially for the long-time aging and device operation. Defect structures, such as fluorenone and excimer trapping sites, always caused long-wavelength emission and nonradiative processing, which are harmful to the efficiency, color purity and stability of deep-blue OLEDs.[30,34] Besides, the unmatched energy level for the fluorene-based OLEDs also cause a serious and bad carrier injection, due to the intrinsic wide bandgap of homo-fluorene with a low highest occupied molecular orbital (HOMO), which also result in a charge accumulation for the large hole-injection barrier, which may also result in a low operation lifetime (Scheme 1).[11,29] To resolve these problems, herein, we demonstrated two novel terfluorenes to explore the role of charge-transport pendant segment (**MC6Cz** and **MC8**), carbazole (Cz), on the stability and efficiency of the deep-blue solution-processed OLEDs. As we expected, **MC6Cz** and **MC8** spin-coated films showed deep-blue emission with a PLQY of ~60%. More interestingly, compared to **MC8** ones, **MC6Cz** spin-coated films show a relatively stable and narrowband deep-blue emission without obvious green-band emission after keeping it in air atmosphere (~3 h). OLEDs based on the **MC6Cz** had a maximum external quantum efficiency (EQE) of 1.17% and CIE coordinates of (0.16, 0.06). Furthermore, **MC6Cz**-based OLEDs also had a longer operation lifetime and stable color purity stability than those of **MC8**, revealing that the introduction of the pendant Cz segment is useful to improve the efficiency and operation lifetime of deep-blue OLEDs.

Results and discussion

According to previous work, the controlled **TFPC0**, as shown in Scheme 1d, had an unwanted green emission band range from 500–700 nm, resulting in a lower color purity of the deep-blue emission.[35] The flexible side-chain substitution at the 4-position of terfluorene may not only improve the solubility to enhance the film-forming ability *via* solution processing technology but also suppress intermolecular aggregation toward obtaining deep-blue emission. In addition, the introduction of the pendant Cz group at the 4-position can also establish a charge-transport channel to enhance the film conductivity (Scheme 1e).[36] The chemical structures of these two deep-blue luminescent materials are shown in Scheme 1d. Building on our previous work, the main monomers were synthesized by a major Baeyer–Villiger rearrangement reaction.[36,37] Then, two compounds of **MC6Cz** and **MC8** were prepared by the Suzuki coupling reaction, and the detailed synthetic procedures are described in the ESI† (Scheme S1); their chemical structures were further verified by nuclear magnetic resonance (NMR) spectroscopy, mass spectra and single crystal data (Fig. S1–S6, ESI†). Decomposition temperatures (T_d) (corresponding to 5% weight loss) of **MC6Cz** and **MC8** were found to be 328 °C, and 388 °C, respectively, by thermogravimetric analysis (TGA) (Fig. S7a and b, ESI†). Two compounds exhibit high T_d, indicating their remarkable thermal stability. In addition, according to

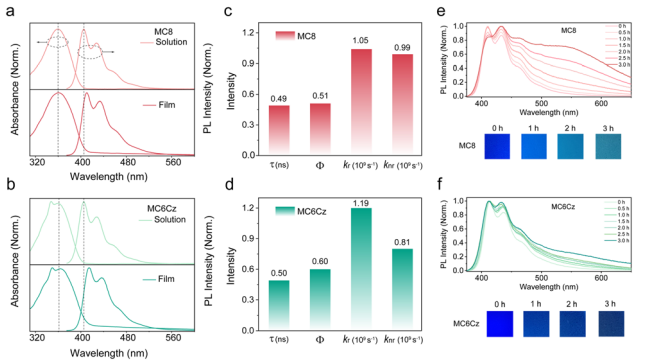

Fig. 1 Optical property of **MC8** and **MC6Cz**. Absorption and PL spectra of **MC8** (a) and **MC6Cz** (b) in solutions and spin-coated films from toluene solutions. Fluorescence lifetime, photoluminescence quantum yield, radiative and non-radiative transition rates ($k_r = \Phi/\tau$, $k_{nr} = 1/\tau - k_r$) of **MC8** (c) and **MC6Cz** (d) spin-coated films. PL spectra of **MC8** (e) and **MC6Cz** (f) aged films. The aged films were prepared by continuous irradiation of spin-coated films under a 365 nm UV lamp.

differential scanning calorimetry (DSC), the glass transition temperatures (T_g) of the **MC6Cz** and **MC8** were 133 °C and 105 °C, respectively (Fig. S7c and d, ESI†). The T_g of **MC6Cz** is higher than that of **MC8**, which is due to the pendant Cz group restricting the movement between molecules. Simultaneously, the two materials are soluble in toluene, dichloromethane and other common organic solvents, and the preparation of the uniform film ensures solution processability in the preparation of OLED devices. Uniform and stable films as well as good thermal stability allow for proper operation of the optoelectronic devices.

Firstly, the photophysical behaviour of the two compounds in solution and the thin film was further investigated, including techniques such as steady UV-*vis* absorption, PL spectra, time-resolved fluorescence emission decays spectra and transient absorption (TA) analysis. As displayed in Fig. 1a and b, for the absorption spectra of a dilute solution, **MC8** has an absorption peak at 360 nm, and **MC6Cz** has two absorption peaks at 348 nm and 360 nm. The former absorption peak for **MC6Cz** is attributed to the carbazole. For the PL spectra of the dilute solution, the two materials have three emission peaks with the same characteristics at 405 nm, 428 nm, and 460 nm, due to the singlet transition within the chromophore 0–0, 0–1, 0–2 of the conjugated structure. The absorption spectra of the two materials' spin-coated films are similar to those of the dilute solution, indicating no significant molecular aggregation behaviour in the film.[16,30] Compared with the dilute solution, the PL spectra of the spin-coated films have a smaller red-shift, attributed to the constraints of intramolecular conformational motion. Meanwhile, the emission peaks of **MC8** spin-coated film are at 410 nm, 434 nm, 465 nm, and those of **MC6Cz** films are estimated at 415 nm, 437 nm, and 470 nm, consistent with the corresponding PL-mapping plots in Fig. S8 (ESI†). Correspondingly, the CIE coordinates of both materials are about (0.16, 0.06). The results show that it has excellent ultra-deep-blue emission behaviour and can be used in the field of information display. In addition, the lifetime and fluorescence quantum efficiency of the two material films were studied by time-resolved transient PL measurements. The lifetimes of **MC8** and **MC6Cz** were calculated as 0.49 ns and 0.50 ns (Fig. S9, ESI†). More importantly, the fluorescence quantum efficiency of **MC8** and **MC6Cz** were estimated to be 51.27% and 59.51%, also revealing a robust deep-blue emission. Their radiative and non-radiative transition rates were calculated, as shown in Fig. 1c and d. A higher radiative transition rate and a lower non-radiative transition rate of **MC6Cz**, indicate that the carbazole group effectively inhibits the non-radiative transition of excitons and improves excitons utilization, which also reasonably explains the higher fluorescence quantum efficiency of **MC6Cz** than those of **MC8**.

In order to research the film formation of these compounds, the spin-coated films were subjected to XRD morphological characterization. Both of the spin-coated films exhibit relatively wide random scattering peaks (Fig. S11, ESI†), suggesting the amorphous states in the solid films. To further investigate the emission spectral stability, the thermal annealing and aging treatments of their spin-coated films were subjected to both materials. Spin-coated film was thermally annealed at 120 °C in the air for different times (Fig. S10, ESI†), no significant changes in the PL spectra were observed at different annealing times, and no green light band at 500–550 nm were discovered for their annealed films, evidencing that two materials have good deep-blue PL spectral stability. Then, the spin-coated films of the two materials were also exposed to a 365 nm UV lamp for 3 h for the continuous aging experiment. Surprisingly, a clear peak at 550 nm appeared for the **MC8** aged films at 1.5 hours of continuous irradiation under a UV lamp, while there is no obvious green-band emission for **MC6Cz** even at 3 hours of irradiation, also effectively suggesting that the suppression of green-band emission by pendant carbazole units (Fig. 1e and f). What is more, as can be seen from the photographs that the colour of the **MC8** film changes significantly under UV lamp irradiation, to blue-green emission after 2.0 hours, while the **MC6Cz** film has a slight change in colour, remaining pure blue emission after 3 h. From the above results, compared to **MC8**, **MC6Cz** presents excellent deep-blue spectral stability. In summary, the introduction of Cz groups, steric hindrance functionalization of the fluorene main chain, barrier layer in the conjugated main chain, reduced Stokes shift, enabling the molecular level coating of luminous color groups and inhibiting the aggregation between molecular main chains, realizes the exciton behavior of single molecule mechanism and improve the morphological and spectral stability of the film. At the same time, the non-radiative transition of excitons can be effectively inhibited, the utilization rate of excitons can be improved, and the generation of the green band can be inhibited, which is conducive to the realization of efficient and stable solution-processable deep-blue light-emitting devices.

The intermolecular interaction and aggregation always affect the dynamical behavior of excited states and excitons. We further investigated the behaviour of excitons in films of **MC6Cz** and **MC8** by femtosecond transient absorption

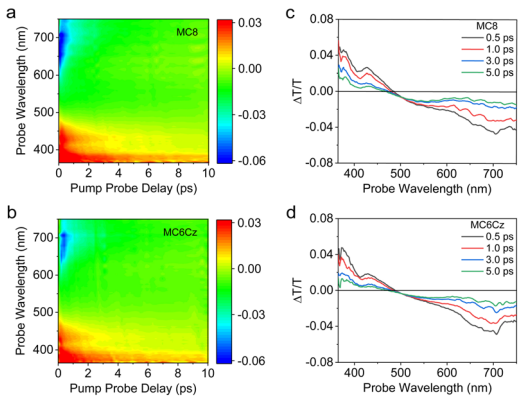

Fig. 2 Transient absorption (TA) analysis of **MC8** and **MC6Cz** films. TA contour plots of **MC8** (a) and **MC6Cz** (b). (c) and (d) $\Delta T/T$ spectra of **MC8** and **MC6Cz** films from 0.5 to 5.0 ps pump–probe delay.

spectroscopy. Fig. 2a and b show TA contour plots of the two types of spin-coated films in the 350 to 750 nm. Both contour plots consist of three distinct regions, where the positive signal in the 350–410 nm spectral range (red region) shows photobleaching (PB), consistent with the absorption spectra of the film. The 410–480 nm spectral range (red region) is attributed to stimulated emission (SE), consistent with the emission spectra of the films. The negative signal at long wavelengths (blue region) is associated with photoinduced absorption (PA). The differential transmission ($\Delta T/T$) spectra of two material spin-coated films at the probe delay time are in Fig. 2c and d. The spectra of the two materials showed similar trends over the entire time scale. The PB and PA signals of **MC6Cz** are both stronger than **MC8**, indicating that the excited state excitons of **MC6Cz** are reabsorbed, which improves the utilization rate of the exciton. In addition, the $\Delta T/T$ zero-crossing point of **MC6Cz** is red-shifted relative to **MC8**, indicating that the formation of polariton pairs in **MC6Cz** is effectively suppressed, showing single-molecule emission, which explains the low non-radiative transition of **MC6Cz**. Furthermore, the SE and PA kinetic traces (Fig. S12, ESI†) have perfect symmetric $\Delta T/T$ behaviour, further confirming their single-molecule exciton emission in the film.

To obtain a deep understanding of this pendant functionalization on the electronic structure, we also performed DFT calculations of both compounds and obtained the optimized structure and the molecular orbitals of the highest occupied (HOMO) and lowest unoccupied (LUMO), as shown in Fig. S13 (ESI†). The large dihedral angle between diphenyls at the 9 positions of the fluorene, and this structure is effective in reducing aggregation caused by intermolecular interactions, which is conducive to improving deep-blue emission and their stability. In addition, it also concluded that the pendant Cz group is slightly influenced by the photophysical processing of the terfluorene backbone structures, which is beneficial for obtaining single-chromophore emission behavior. Besides, the calculated HOMO and LUMO energy levels of the **MC8** and **MC6Cz** are −5.14 eV and −1.45 eV, −5.25 eV and −1.54 eV, respectively, indicating the narrow energy gaps for deep-blue emission. The electrochemical properties of the materials were characterized by CV (Fig. S14, ESI†). The HOMO and LUMO of the materials were calculated from HOMO/LUMO = $-[E_{onset} - E(Fc/Fc^{+}) + 4.8]$ eV. The onset of the oxidation potential (E_{ox}) for **MC8** and **MC6Cz** are 1.46 eV and 1.14 eV, and their onset of reduction potential (E_{red}) are −1.85 eV and −1.93 eV, respectively. As a result, the HOMO and LUMO energy levels for **MC8** and **MC6Cz** are −5.79 eV and −2.48 eV, −5.48 eV and −2.40 eV, respectively. Therefore, the introduction of the pendant Cz units can increase the HOMO energy level to ensure the hole injection from the hole-transporting layer (HTL, such as PEDOT: PSS) and avoid charge accumulation (as shown in Scheme 1a), effectively improving the efficiency and stability of OLEDs.

The stability of the thin film morphology is very important for the fabrication and performance of the device, so the spin-coated films were subjected to FLM and AFM morphological characterization. As shown in Fig. 3e and g, both spin-coated films (40–50 nm) present smooth and particle-free surface morphology, with RMS roughness of 0.261 nm, and 0.302 nm for **MC8** and **MC6Cz**, respectively. The roughness of **MC6Cz** is slightly higher than that of **MC8**, mainly due to the increased entanglement of the molecular chains by the Cz group. In addition, the surface morphologies of their annealed films were characterized by AFM measurements (Fig. 3f and h), and RMS was estimated to be about 0.276 nm, 0.332 nm of **MC8** and **MC6Cz** annealed film. The roughness of the spin-coated films is slightly changed after thermal annealing, indicating that they have good film morphological stability. At the same time, the FLM images (Fig. 3a–d) of the pristine film as well as the annealed film of both materials also show smooth and particle-free surfaces, and the annealed films are intact without significant changes. Therefore, the two materials have good thin film morphology and stability, and have good ability to fabricate devices by solution processing. Due to their ultra-deep blue emission, excellent film morphology, good spectral stability, and excellent solubilizable properties, these two materials can be used as candidate emission materials for deep-blue solution-processed OLEDs. Subsequently, preliminary single-layer OLEDs are fabricated with a traditional configuration of ITO/PEDOT:PSS

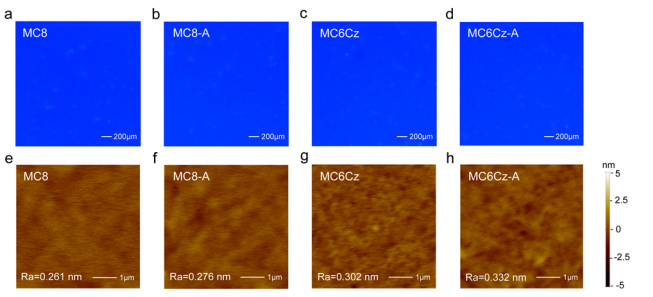

Fig. 3 Fluorescence microscope (FLM) and atomic force microscopy (AFM) images of pristine films of **MC8** (a) and (e), **MC6Cz** (c) and (g), annealed films of **MC8** (b) and (f), **MC6Cz** (d) and (h). The annealed film was prepared after thermal treatments at 120 °C in a nitrogen atmosphere for 15 min.

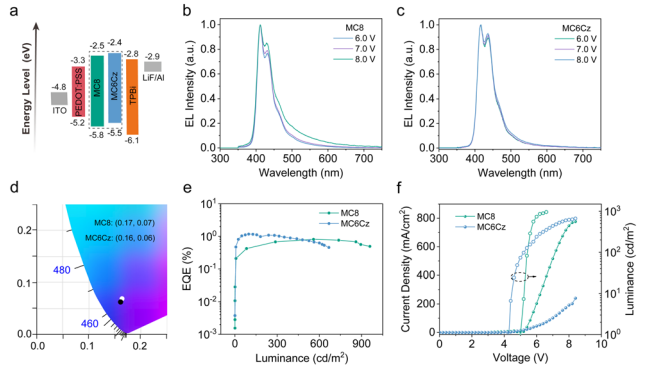

Fig. 4 Configuration structure and performance of OLEDs based on **MC8** and **MC6Cz** film. (a) Energy levels of OLEDs based on **MC8** and **MC6Cz**. Electroluminescence (EL) spectra of **MC8** (b) and **MC6Cz** (c). (d) CIE chromaticity coordinate of **MC8** and **MC6Cz**. EQE *versus* luminance (e) and current density–luminance–voltage (f) curves of the devices.

(40 nm)/emission layer (EML, 45 nm)/TPBi (20 nm)/LiF (1 nm)/Al (100 nm), as shown in Fig. 4a. As expected, EL spectra of OLEDs based on **MC8** and **MC6Cz** consisted of 410 nm and 434 nm, 415 nm and 437 nm, respectively, similar to their PL spectra, as shown in Fig. 4b and c, indicating extremely weak interchain aggregation. More importantly, both two OLEDs exhibited narrowband deep-blue emission with an FWHM of <50 nm. Besides, with the increase of applied voltage, in contrast to **MC8** ones, OLEDs based on **MC6Cz** exhibit a stable EL spectral profile without an obvious emission peak at 500–600 nm, confirming the good deep-blue emission spectral stability. Corresponding CIE values of the **MC8** and **MC6Cz** (Fig. 4d) are (0.17, 0.07) and (0.16, 0.06), respectively, suggesting the ultra-deep blue emission. As shown in Fig. 4e, current efficiency *versus* luminance curves, the maximum external quantum efficiency (EQE) values of **MC8** and **MC6Cz** were estimated at about 0.76% and 1.17%, respectively. As we expected, **MC6Cz** has a relatively high EQE, indicating that the carbazole group improves the carrier mobility of the materials. Meanwhile, the turn-on voltages of **MC8** and **MC6Cz** are estimated at about 5.0 V and 4.2 V respectively (Fig. 4f), indicating a better charge injection and high conductivity of the **MC6Cz** emission layers. Besides, the maximum luminance of **MC8** and **MC6Cz** is about 959 cd m^{-2} and 667 cd m^{-2}, respectively. More interestingly, **MC6Cz**-based OLED presents a high brightness at low current densities, attributed to the hole transport properties and matched energy level of carbazole. In addition, the **MC6Cz**-based OLEDs also have a longer operation time and stable color purity than those of **MC8** (Fig. S16, ESI†), which also reveals that the introduction of a pendant Cz segment improves the efficiency and operation stability of deep-blue OLEDs. Because the Cz side group substituents can form an ordered stacked structure and form a new carrier transport channel, which can effectively improve the carrier transport characteristics and has important significance for improving the performance and efficiency of the device. Meanwhile, the relatively high and stable deep-blue emissions of **MC6Cz** in the coated films are also good for improving the device efficiency of OLEDs.

Conclusions

In summary, a series of 4-position functionalized steric terfluorenes were designed and prepared *via* pendant side-functionalization for spectrally stable solution-processed deep-blue OLEDs. Based on the time-resolved transient spectroscopy, both materials exhibit efficient deep-blue emission in the film states, associated with the single-molecular excitonic behavior. More interestingly, compared to **MC8**, **MC6Cz** has a relatively high PLQY of 60% and stable deep-blue emission, even after aging under UV excitation, due to their self-encapsulation. Furthermore, **MC6Cz**-based OLEDs displayed a narrow band deep-blue emission with a maximum EQE of 1.17%, and CIE coordinates of (0.16, 0.06). Compared to **MC8**, **MC6Cz**-based OLEDs also had a long operation time and stable deep-blue luminescence. Therefore, the introduction of a pendant Cz segment is an effective tool for improving the efficiency and stability of deep-blue OLEDs.

Conflicts of interest

There are no conflicts to declare.

Acknowledgements

This work is financially supported by the National Key R&D Program of China (No. 2020YFA0709900); W. Huang, J. Lin, B. Liu, L. Bai, and Y. Han acknowledge support from the National Natural Science Foundation of China (No. 62288102, 61874053, 22075136, 22105099, 62105262, and 62205141); Y. Han and L. Bai thank the China Postdoctoral Science Foundation (No. 2022M711591 and 2021M692623); X. An acknowledges support from Jiangsu Funding Program for Excellent Postdoctoral Talent; All authors discussed the results and commented on the manuscript at all stages.

Notes and references

1 J. H. Burroughes, A. R. Brown, R. N. Marks, K. Mackay, R. H. Friend, P. L. Burns and A. B. Holmes, Light-emitting diodes based on conjugated polymers, *Nature*, 1992, **347**, 539.
2 S. Reineke, F. Lindner, G. Schwartz, N. Seidler, K. Walzer, B. Lüssem and K. Leo, White organic light-emitting diodes with fluorescent tube efficiency, *Nature*, 2009, **459**, 234–238.
3 Z. Zhang, W. Wang, Y. Jiang, Y.-X. Wang, Y. Wu, J.-C. Lai, S. Niu, C. Xu, C.-C. Shih, C. Wang, H. Yan, L. Galuska, N. Prine, H.-C. Wu, D. Zhong, G. Chen, N. Matsuhisa, Y. Zheng, Z. Yu, Y. Wang, R. Dauskardt, X. Gu, J. B. H. Tok and Z. Bao, High-brightness all-polymer stretchable LED with charge-trapping dilution, *Nature*, 2022, **603**, 624–630.
4 M. S. White, M. Kaltenbrunner, E. D. Głowacki, K. Gutnichenko, G. Kettlgruber, I. Graz, S. Aazou, C. Ulbricht, D. A. M. Egbe, M. C. Miron, Z. Major, M. C. Scharber, T. Sekitani, T. Someya, S. Bauer and N. S. Sariciftci, Ultrathin,

highly flexible and stretchable PLEDs, *Nat. Photonics*, 2013, **7**, 811–816.
5 G. Pacchioni, Light my firefly, *Nat. Rev. Mater.*, 2016, 16030.
6 H. Ling, S. Liu, Z. Zheng and F. Yan, Organic Flexible Electronics, *Small Methods*, 2018, **2**, 1800070.
7 J. Harding, OLCD: Delivering an Exciting Future for Flexible Displays, *Inf. Disp.*, 2019, **35**, 9–13.
8 Y. G. Huang, E. L. Hsiang, M. Y. Deng and S. T. Wu, Mini-LED, Micro-LED and OLED displays: present status and future perspectives, *Light-Sci. Appl.*, 2020, **9**, 105.
9 J. Y. Woo, M. H. Park, S. H. Jeong, Y. H. Kim, B. Kim, T. W. Lee and T. H. Han, Advances in Solution-Processed OLEDs and their Prospects for Use in Displays, *Adv. Mater.*, 2023, **35**, 2207454.
10 J. H. Lee, C. H. Chen, P. H. Lee, H. Y. Lin, M. K. Leung, T. L. Chiu and C. F. Lin, Blue organic light-emitting diodes: current status, challenges, and future outlook, *J. Mater. Chem. C*, 2019, **7**, 5874–5888.
11 S. S. Swayamprabha, D. K. Dubey, R. A. K. Yadav, M. R. Nagar, A. Sharma, F. C. Tung and J. H. Jou, Approaches for Long Lifetime Organic Light Emitting Diodes, *Adv. Sci.*, 2021, **8**, 2002254.
12 P. E. Shaw, A. Ruseckas, J. Peet, G. C. Bazan and I. D. W. Samuel, Exciton Annihilation in Mixed-Phase Polyfluorene Films, *Adv. Funct. Mater.*, 2010, **20**, 155–161.
13 C. Ou, N. J. Cheetham, J. Weng, M. Yu, J. Lin, X. Wang, C. Sun, J. Cabanillas-Gonzalez, L. Xie, L. Bai, Y. Han, D. D. C. Bradley and W. Huang, Hierarchical Uniform Supramolecular Conjugated Spherulites with Suppression of Defect Emission, *iScience*, 2019, **16**, 399–409.
14 T. Nakamura, D. K. Sharma, S. Hirata and M. Vacha, Intrachain Aggregates as the Origin of Green Emission in Polyfluorene Studied on Ensemble and Single-Chain Level, *J. Phys. Chem. C*, 2018, **122**, 8137–8146.
15 X. T. Hao, L. J. McKimmie and T. A. Smith, Spatial Fluorescence Inhomogeneities in Light-Emitting Conjugated Polymer Films, *J. Phys. Chem. Lett.*, 2011, **2**, 1520–1525.
16 F. Cacialli, J. S. Wilson, J. J. Michels, C. Daniel, C. Silva, R. H. Friend, N. Severin, P. Samorì, J. P. Rabe, M. J. O'Connell, P. N. Taylor and H. L. Anderson, Cyclodextrin-threaded conjugated polyrotaxanes as insulated molecular wires with reduced interstrand interactions, *Nat. Mater.*, 2002, **1**, 160–164.
17 R. Noriega, J. Rivnay, K. Vandewal, F. P. V. Koch, N. Stingelin, P. Smith, M. F. Toney and A. Salleo, A general relationship between disorder, aggregation and charge transport in conjugated polymers, *Nat. Mater.*, 2013, **12**, 1038–1044.
18 V. Podzorov, Conjugated Polymers Long and winding polymeric roads, *Nat. Mater.*, 2013, **12**, 947–948.
19 A. C. Grimsdale, P. Leclère, R. Lazzaroni, J. D. Mackenzie, C. Murphy, S. Setayesh, C. Silva, R. H. Friend and K. Müllen, Correlation between molecular structure, microscopic morphology, and optical properties of poly (tetraalkylindenofluorene)s, *Adv. Funct. Mater.*, 2002, **12**, 729–733.
20 M. Knaapila and A. P. Monkman, Methods for controlling structure and photophysical properties in polyfluorene solutions and gels, *Adv. Mater.*, 2013, **25**, 1090–1108.
21 F. C. Spano and C. Silva, H- and J-Aggregate Behavior in Polymeric Semiconductors, *Annu. Rev. Phys. Chem.*, 2014, **65**, 477–500.
22 Y. Han, L. Bai, X. An, M. Xu, C. Wei, Z. Lin, M. Yu, J. Lin, L. Sun, N. Sun, C. Wei, L. Xie, X. Ding, Q. Wei, C. Yin, C. Li, W. Su and W. Huang, Intrinsically Viscoelastic Supramolecular Conjugated Polymer toward Suppressing Coffee-Ring Effect, *CCS Chem.*, 2022, **4**, 3529–3539.
23 X. H. Yu, R. B. Xing, Z. X. Peng, Y. M. Lin, Z. H. Du, J. Q. Ding, L. X. Wang and Y. C. Han, To inhibit coffee ring effect in inkjet printing of light-emitting polymer films by decreasing capillary force, *Chin. Chem. Lett.*, 2019, **30**, 135–138.
24 N. E. Jackson, K. L. Kohlstedt, B. M. Savoie, M. O. de la Cruz, G. C. Schatz, L. X. Chen and M. A. Ratner, Conformational Order in Aggregates of Conjugated Polymers, *J. Am. Chem. Soc.*, 2015, **137**, 6254–6262.
25 J. Tagare and S. Vaidyanathan, Recent development of phenanthroimidazolebased fluorophores for blue organic light-emitting diodes (OLEDs): an overview, *J. Mater. Chem. C*, 2018, **6**, 10138–10173.
26 T. Shan, Y. Liu, X. Y. Tang, Q. Bai, Y. Gao, Z. Gao, J. Y. Li, J. Deng, B. Yang, P. Lu and Y. G. Ma, Highly Efficient Deep Blue Organic Light-Emitting Diodes Based on Imidazole: Significantly Enhanced Performance by Effective Energy Transfer with Negligible Efficiency Roll-off, *ACS Appl. Mater. Interfaces*, 2016, **8**, 28771–28779.
27 Z. Gao, Z. M. Wang, T. Shan, Y. L. Liu, F. Z. Shen, Y. Y. Pan, H. H. Zhang, X. He, P. Lu, B. Yang and Y. G. Ma, High-efficiency deep blue fluorescent emitters based on phenanthro[9,10-d]imidazole substituted carbazole and their applications in organic light emitting diodes, *Org. Electron.*, 2014, **15**, 2667–2676.
28 K. S. Yook and J. Y. Lee, Organic Materials for Deep Blue Phosphorescent Organic Light-Emitting Diodes, *Adv. Mater.*, 2012, **24**, 3169–3190.
29 C. Poriel and J. Rault-Berthelot, Blue Single-Layer Organic Light-Emitting Diodes Using Fluorescent Materials: A Molecular Design View Point, *Adv. Funct. Mater.*, 2020, **30**, 1910040.
30 J. M. Ha, S. H. Hur, A. Pathak, J.-E. Jeong and H. Y. Woo, Recent advances in organic luminescent materials with narrowband emission, *NPG Asia Mater.*, 2021, **13**, 53.
31 L. Seijo, M. de Jong, A. Meijerinka and F. T. Rabouwa, *et al.*, Resolving the ambiguity in the relation between Stokes shift and Huang–Rhys parameter, *Phys. Chem. Chem. Phys.*, 2015, **17**, 16959–16969.
32 X. An, J. H. Yang, M. Xu, L. L. Sun, L. B. Bai, K. Wang, Z. Q. Zhuo, Y. Y. Zheng, J. Y. Lin, X. H. Ding, Y. Y. Liu, L. H. Xie, C. R. Yin and W. Huang, Universal 4-qualifiable fluorene-based building blocks for potential optoelectronic applications, *Chin. Chem. Lett.*, 2022, **33**, 5137–5141.
33 C.-R. Yin, L.-H. Xie, W.-Y. Lai, Q.-L. Fan, W. Huang, L.-H. Xie, C.-R. Yin, W.-Y. Lai, Q.-L. Fan and W. Huang, *Prog. Polym. Sci.*, 2012, **37**, 1192–1264.
34 J. Liang, Y. Qian, L. H. Xie, N. E. Shi, S. F. Chen, X. Y. Deng and W. Huang, Spectral stability of polyfluorene-based semiconductors, *Acta Phys. – Chim. Sin.*, 2010, **26**, 946–963.

35 S. W. L. Zhao, S. Shao, J. Ding, L. Wang, X. Jing and F. Wang, Stable and efficient deep-blue terfluorenes functionalized with carbazole dendrons for solution-processed organic light-emitting diodes, *J. Mater. Chem. C*, 2015, **3**, 8895–8903.

36 J. Lin, B. Liu, M. Yu, X. Wang, Z. Lin, X. Zhang, C. Sun, J. Cabanillas-Gonzalez, L. Xie, F. Liu, C. Ou, L. Bai, Y. Han, M. Xu, W. Zhu, T. A. Smith, P. N. Stavrinou, D. D. C. Bradley and W. Huang, Ultrastable Supramolecular Self-Encapsulated Wide-Bandgap Conjugated Polymers for Large-Area and Flexible Electroluminescent Devices, *Adv. Mater.*, 2019, **31**, 1804811.

37 J.-Y. Lin, W.-S. Zhu, F. Liu, L.-H. Xie, L. Zhang, R. Xia, G.-C. Xing and W. Huang, A Rational Molecular Design of β-Phase Polydiarylfluorenes: Synthesis, Morphology, and Organic Lasers, *Macromolecules*, 2014, **47**, 1001–1007.